GSI Future Project

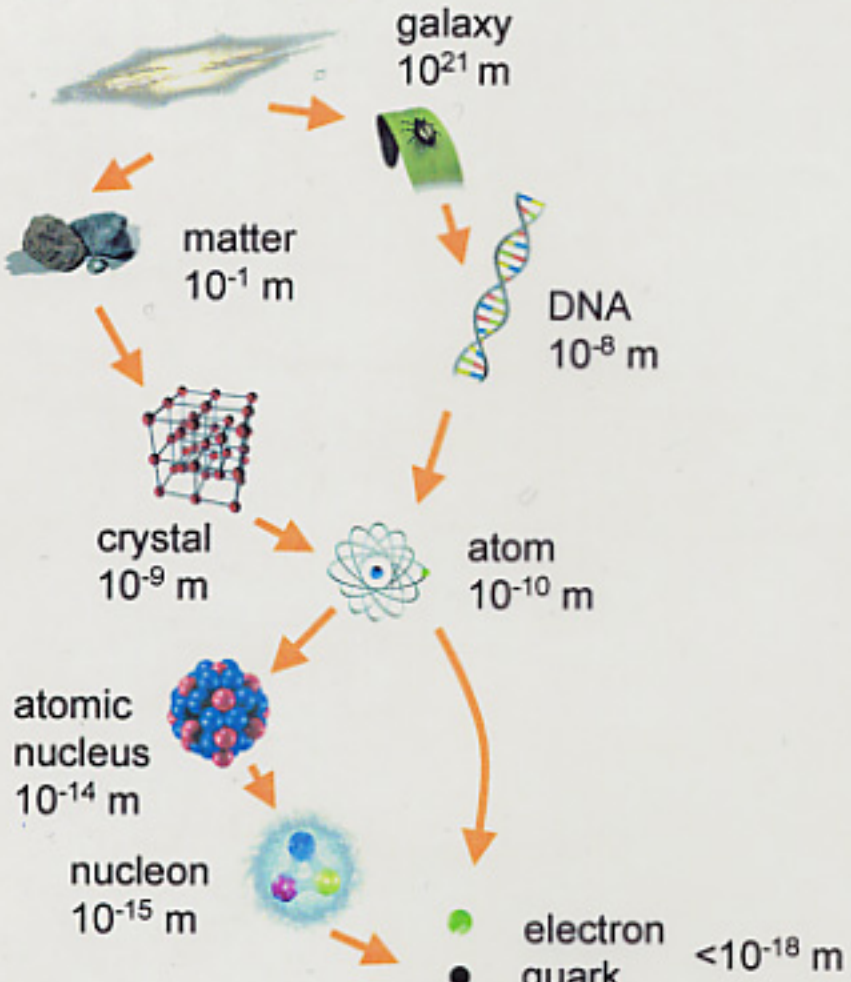

- Plasma physics and physics of high EM fields
- Nuclei far from stability
- Quark-gluon structure of hadrons
- Dense nuclear matter and quark-gluon plasma

- Intense (12 000 GW/g) short (50 ns) HI beam pulses
- 1-1.5 GeV per nucleon beams of shortlived nuclei
- 60 GeV proton beams
- 15 Gev cooled antiproton beams
- 20-30 GeV per nucleon HI beams (U^{93+})

GSI

GSI Future Project

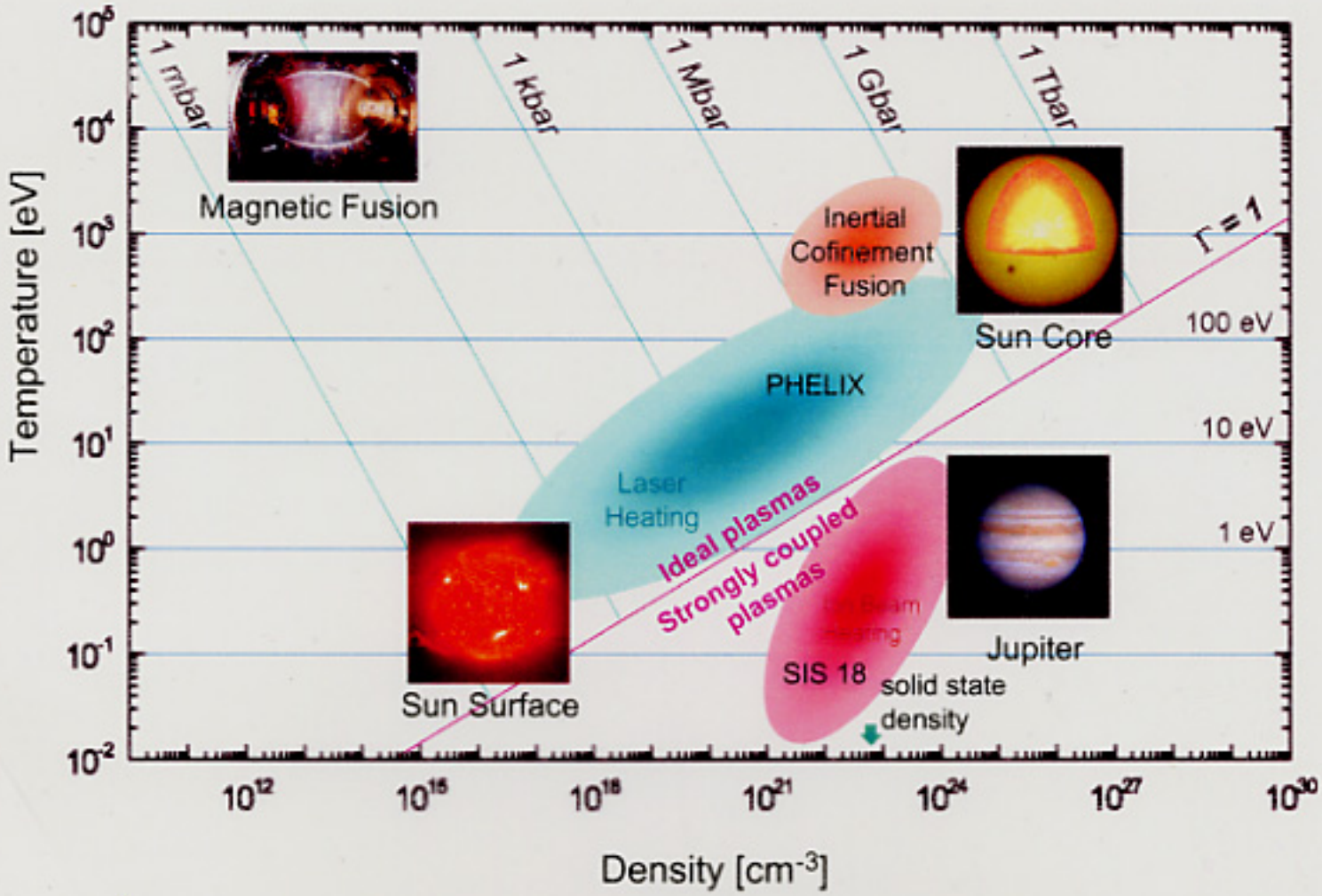

GSI

GSI Future Project

Nuclei at the Extremes

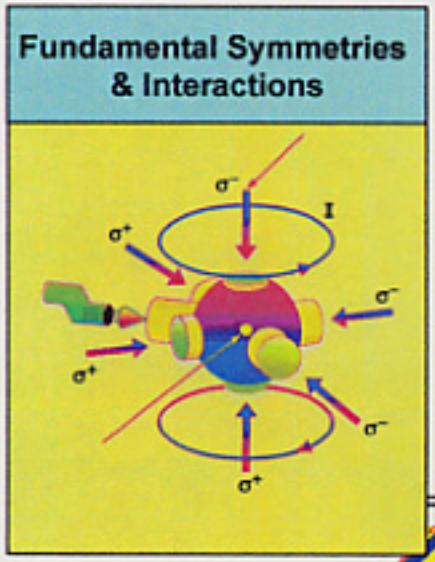

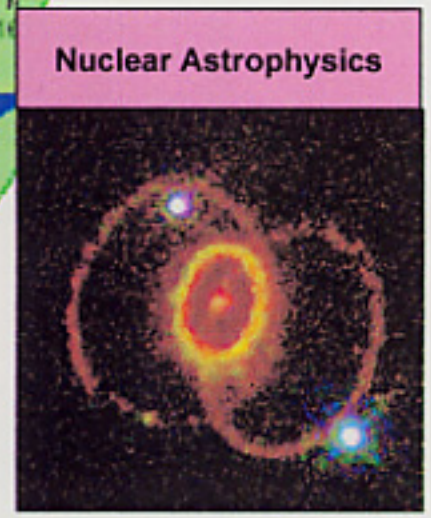

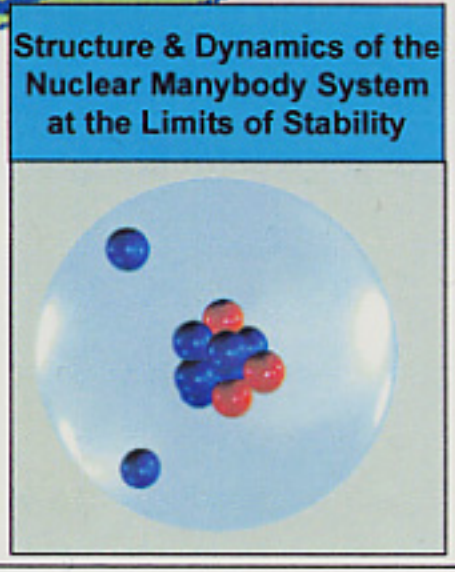

GSI

GSI Future Project

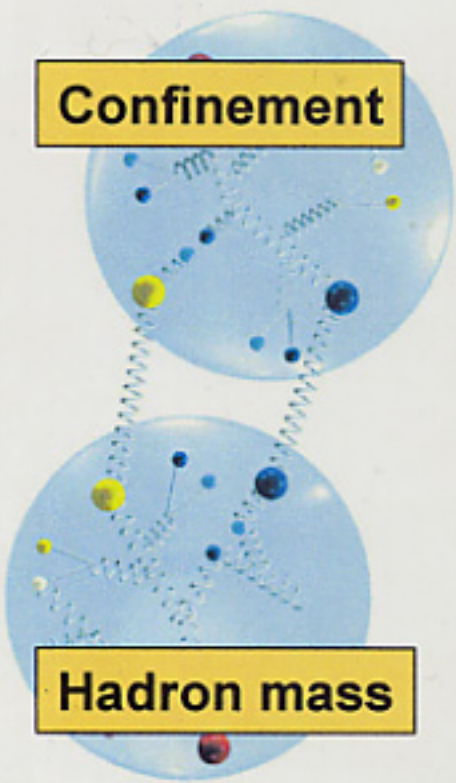

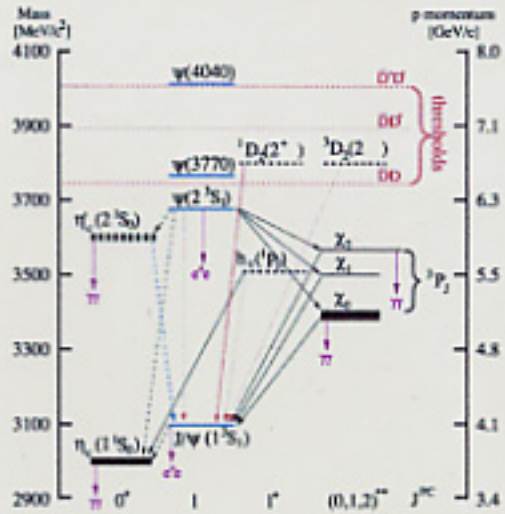

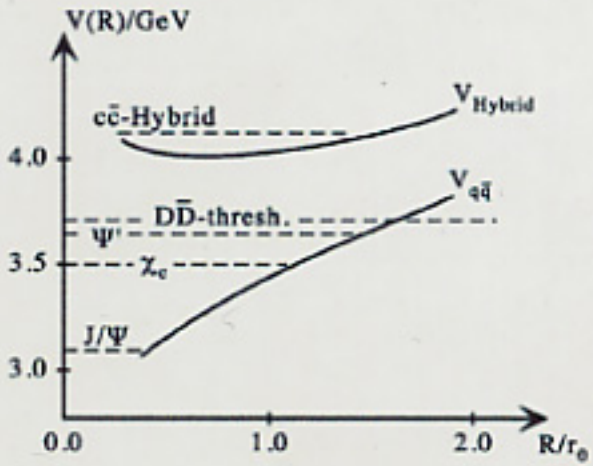

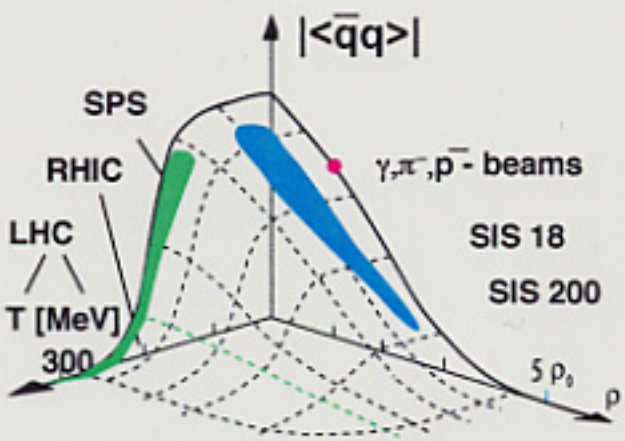

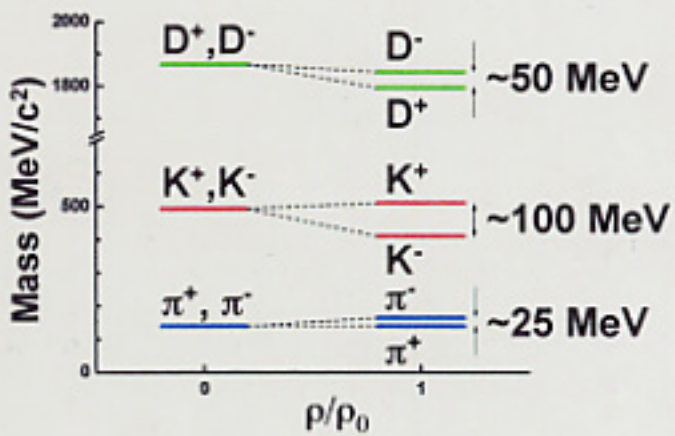

GSI Future Project

Exploring the QCD phase diagram in the region of high baryon densities

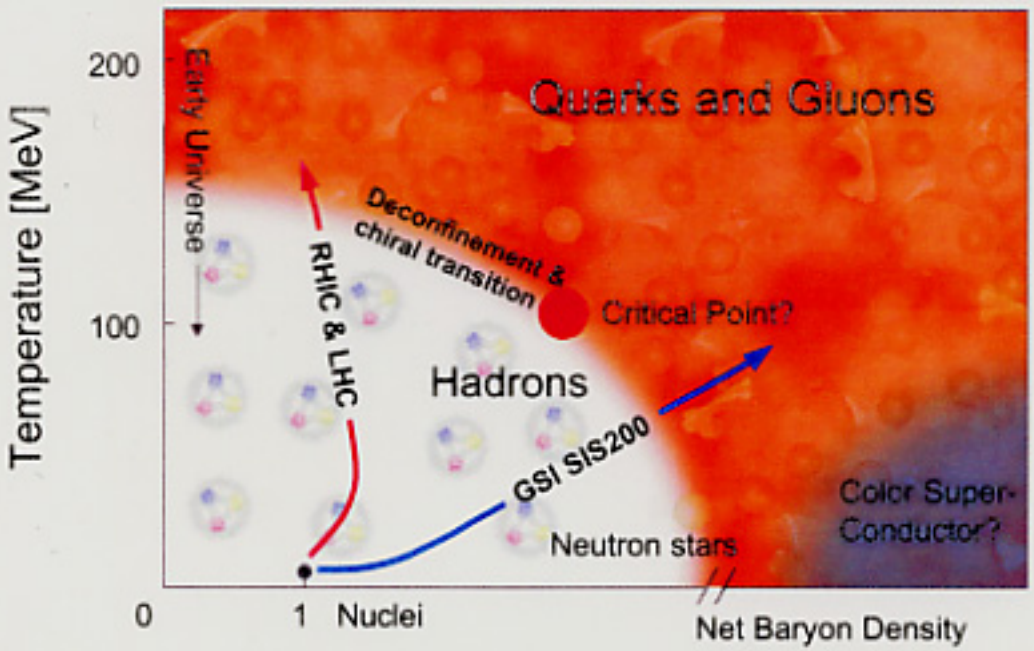

Fundamental questions in strong-interaction physics probed in high energy nucleus-nucleus collisons:

Confinement, broken chiral symmetry and the origin of hadron masses

Experiments search for:

¥Transition from hadronic to quark-gluon matter

¥Restoration of chiral symmetry

¥New states of strongly interacting matter

GSI

GSI Future Project

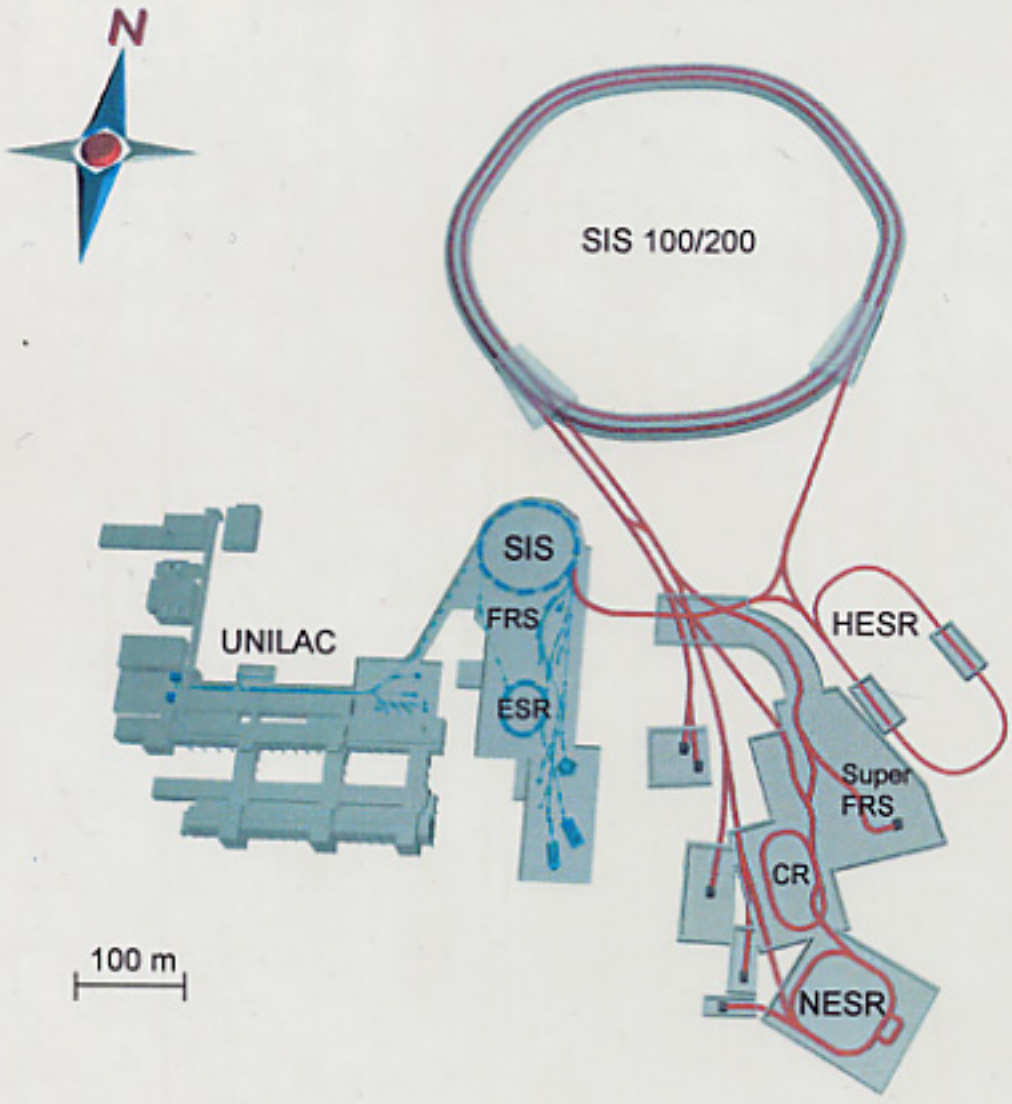

Gain Factors

- Primary beam intensity:
  Factor 100 – 1000
- Secondary beam intensities for radioactive nuclei: up to factor 10,000
- Beam energy: Factor 15

Special Properties

- Intense, fast cooled energetic beams of exotic nuclei
- Cooled antiproton beams up to15 GeV
- Internal targets for high-luminosity in-ring experiments

New Technologies

- Fast cycling superconducting magnets
- Electron cooling at high ion intensities and energies
- Fast stochastic cooling

GSI Future Project

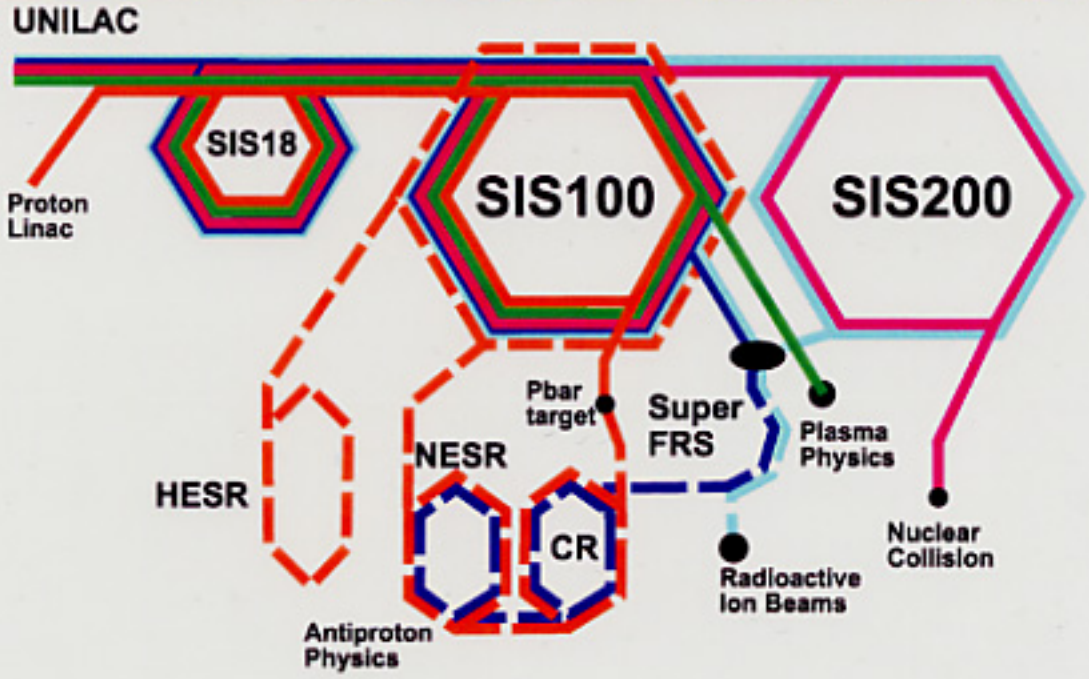

Duty-Cycles of the Accelerator Rings

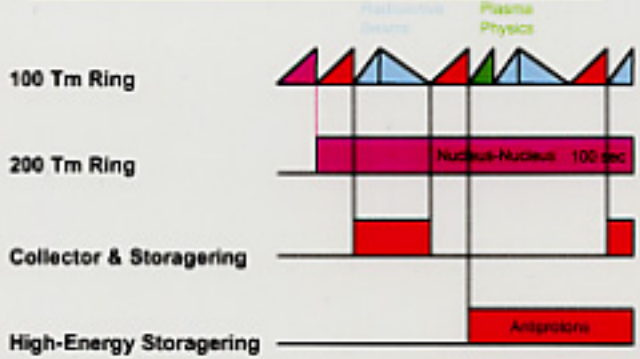

Duty-Cycle of the Physics Programs

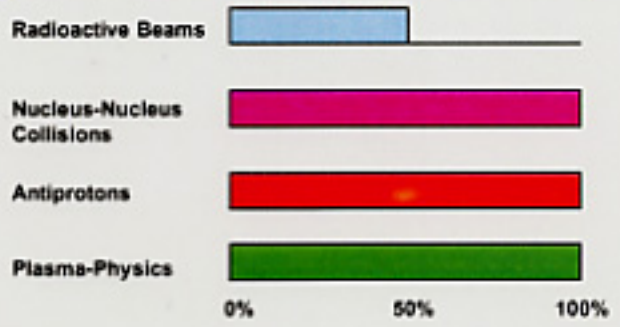

GSI

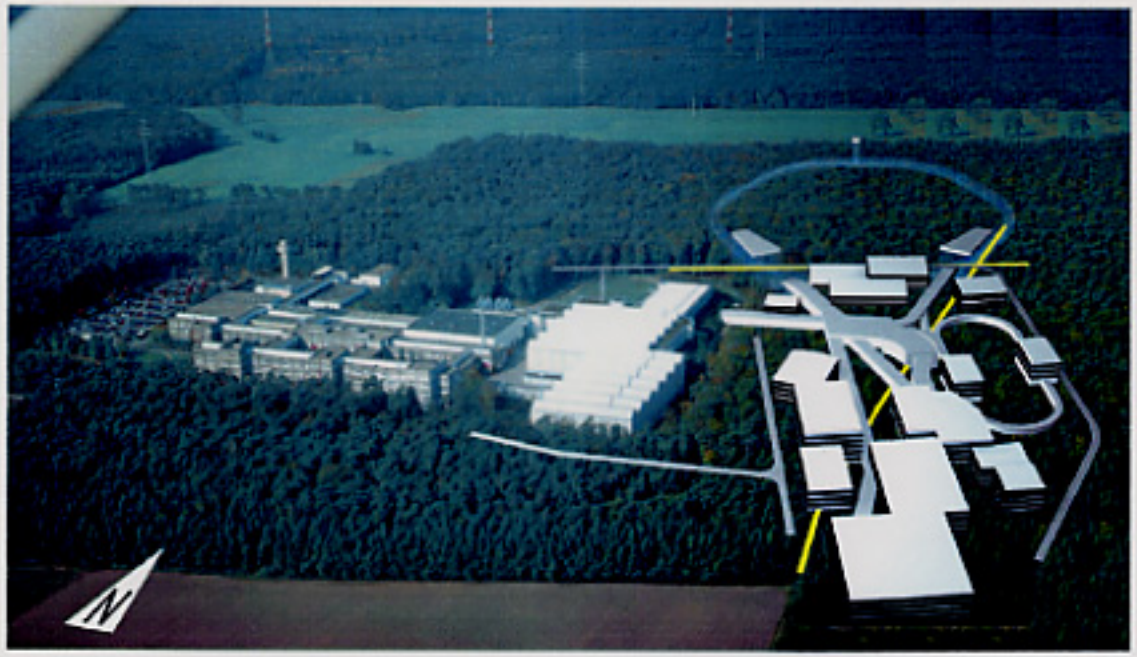

Figure 3.1: Location of the projected new international facility

All of the other buildings and facilities will be arranged south of the large ring tunnel. For these buildings, an above-ground solution is more economical here. The construction of the above-ground buildings will require the clearance of approximately 14 hectares of forest that will be replanted in another area.

COMMUNITY

External peer review and recommendations

External Science Advisory Committee
ESAC

External Technical Advisory Committee
ETAC

Nuclear Physics European Collaboration Committee
NuPECC

Mega-Science Forum
OECD

Users interest

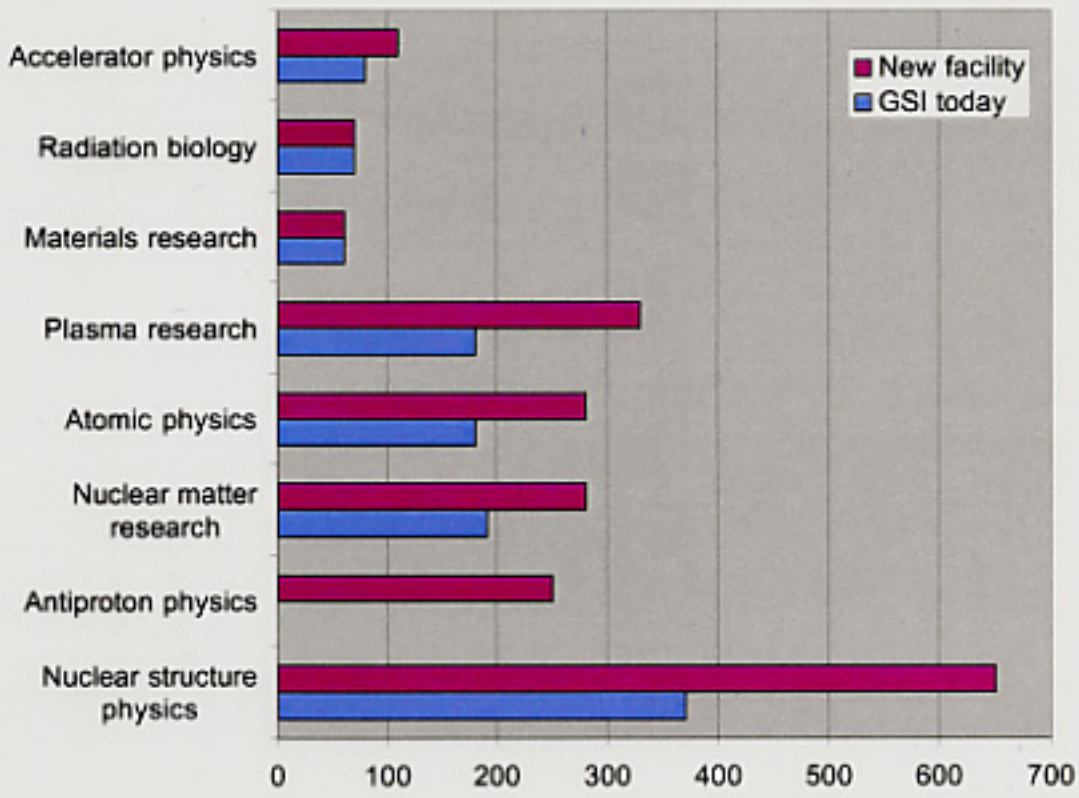

GSI Future Project

COSTS

Building and infrastructure:	225 Mio.
Accelerator:	265 Mio.
Experimental stations / detectors:	185 Mio.
Total:	675 Mio.

SCHEDULE

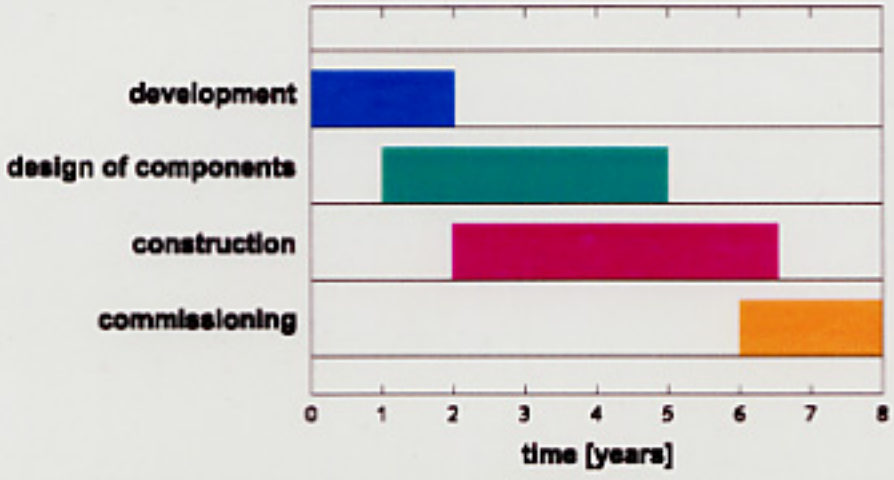

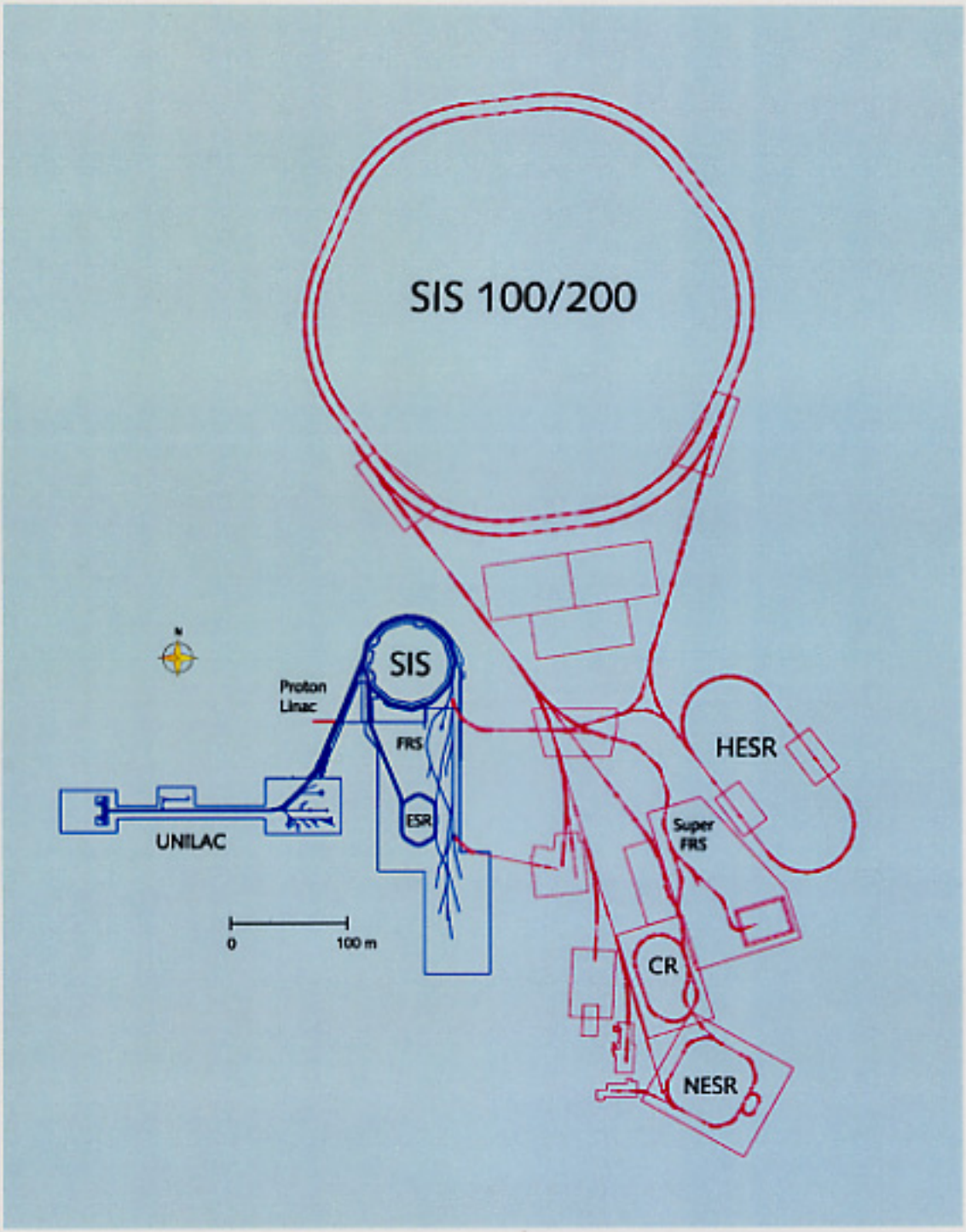

Figure 1: The existing GSI facility (blue) with the linear accelerator UNILAC, the heavy-ion synchrotron SIS18, the fragment separator FRS and the experiment storage ring ESR; and the new project (red) with the double-ring synchrotron SIS100/200, the high-energy storage ring HESR, the collector ring CR, the new experiment storage ring NESR, the super-conducting fragment separator Super-FRS and several experimental stations. The present UNILAC/SIS18 complex serves as injector for the new double-ring synchrotron.

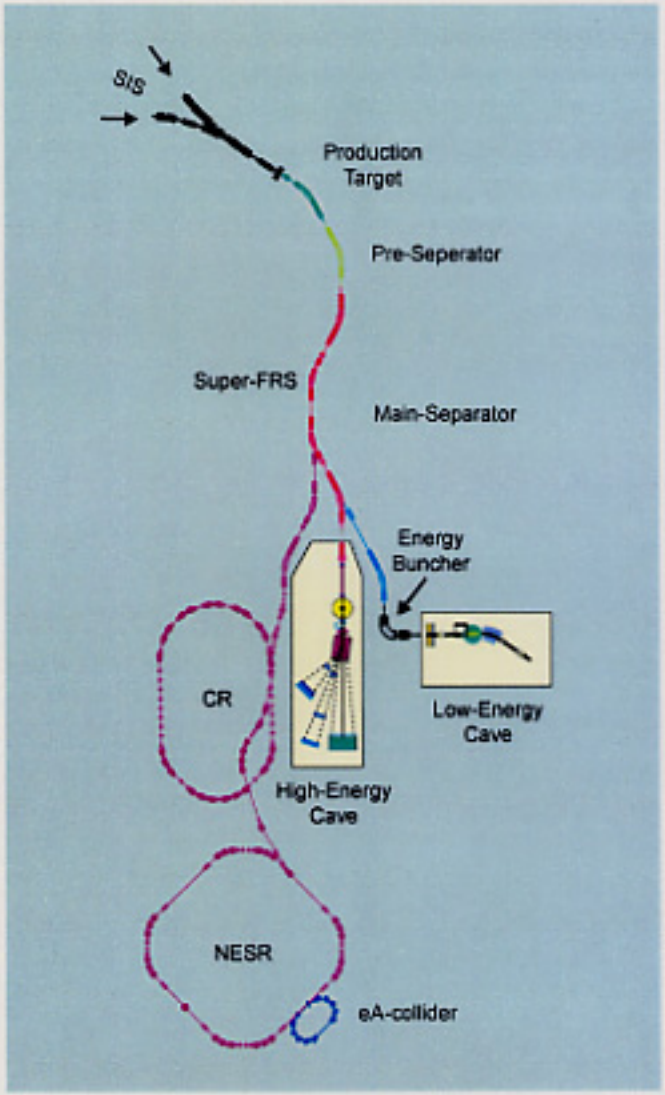

Figure 1.5: Schematic view of the proposed exotic-nuclear-beam facility. The super-conducting two-stage fragment separator (Super-FRS) provides beams of unstable nuclei for the double storage ring system (Collector Ring CR and New Experimental Storage Ring NESR), including an intersecting electron ring (eA collider), as well as for high- and low-energy experimental areas.

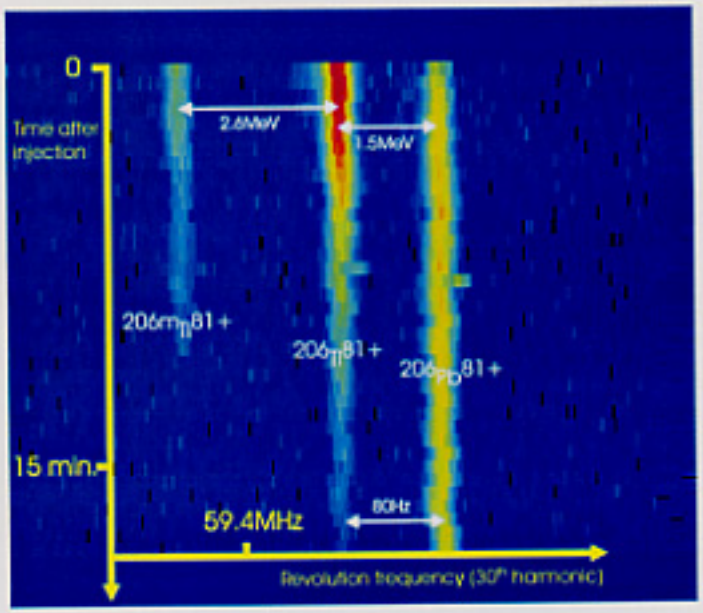

Figure 1.15: First direct observation of bound-state β decay. Bare ^{206}Tl nuclei were produced and separated in the fragment separator FRS, then injected into the ESR, where they were stored and electron-cooled. Displayed is the time evolution of three Schottky lines which correspond, from left to right, to bare ^{206}Tl in an isomeric nuclear state, bare ^{206}Tl in the nuclear ground state, and to the bound-state β-decay daughter of bare ^{206}Tl, i.e. hydrogen-like ^{206}Pb $^{81+}$.

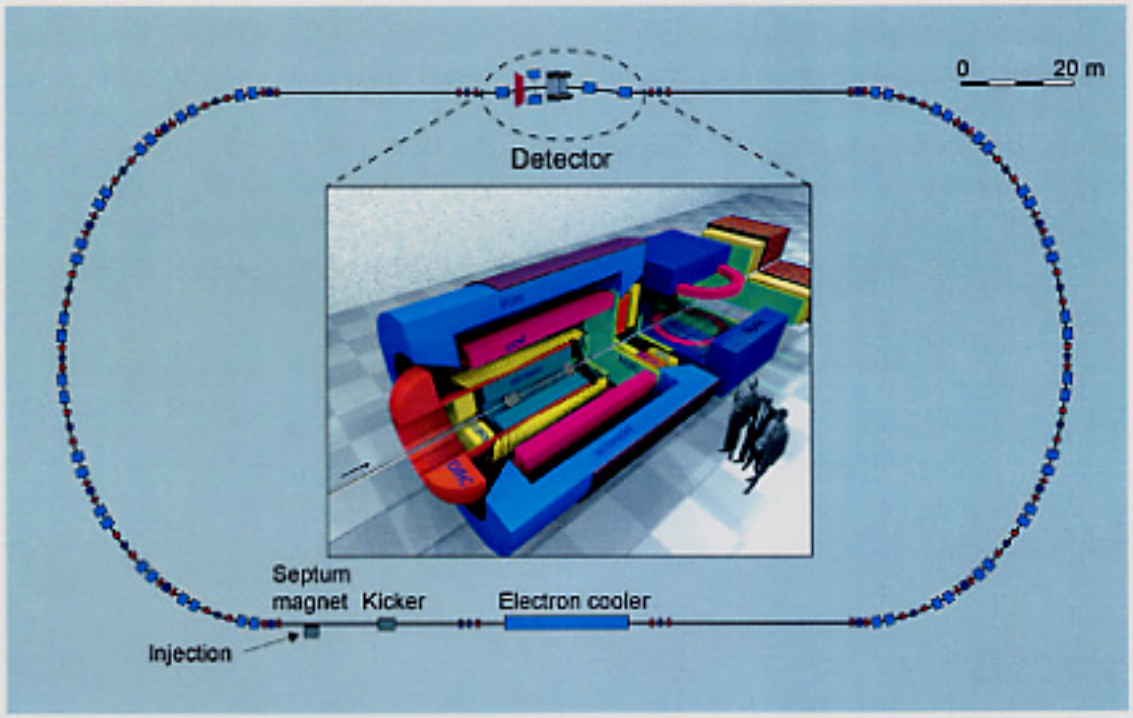

Figure 1.7: Layout of the High-Energy Storage Ring (HESR) with the electron cooler and the almost hermetic detector system at the internal target position.

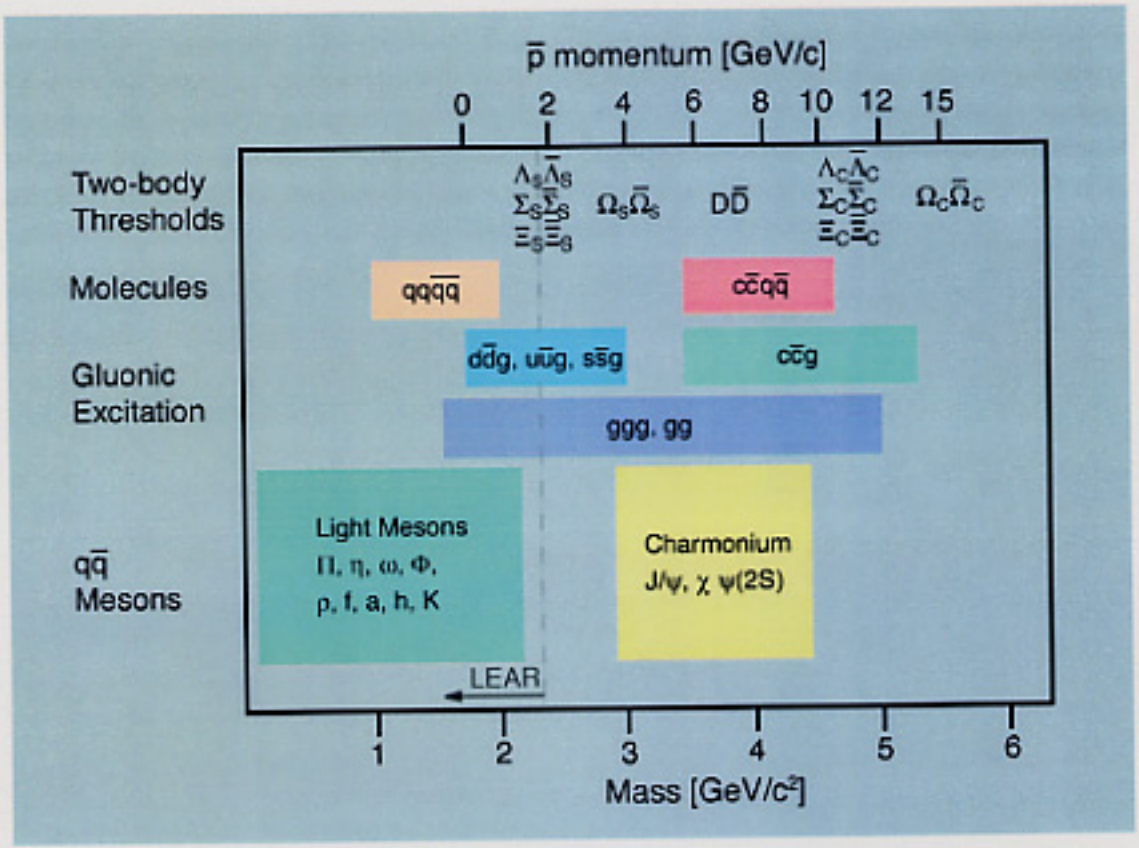

Figure 1.6: Mass range of hadrons accessible at the HESR with antiproton beams. The figure indicates the antiproton momenta required for charmonium spectroscopy, the search for charmed hybrids and glueballs, the production of D meson pairs and the production of Ξ baryon pairs for hypernuclear studies. The energy range covered by the former Low Energy Antiproton Ring (LEAR) at CERN is indicated by the arrow.

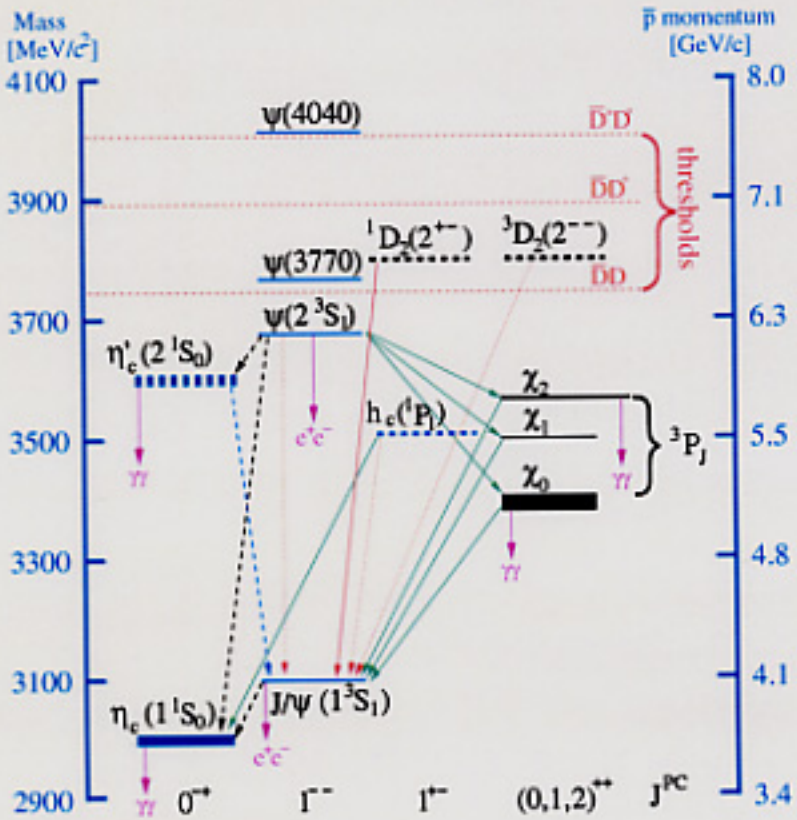

Figure 2.4. Charmonium states and their decay modes. Undiscovered and poorly known states are marked by dashes.

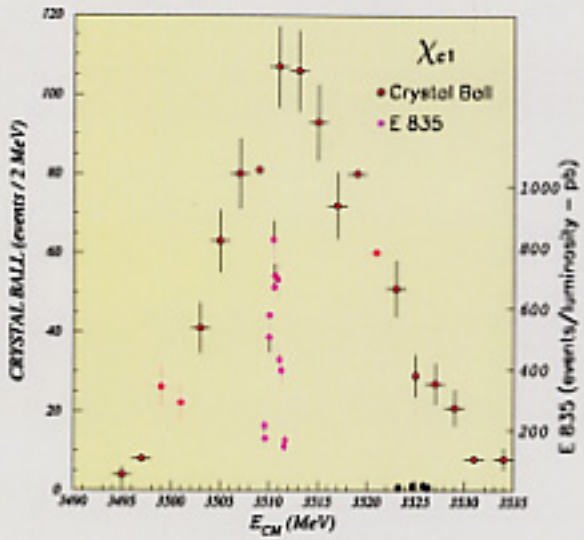

Figure 2.5. Comparison of measurements of the χ_{c1} resonance obtained by e^+e^- annihilation (Crystal Ball, SLAC) and by $\bar{p}p$ annihilation (E835, Fermilab).

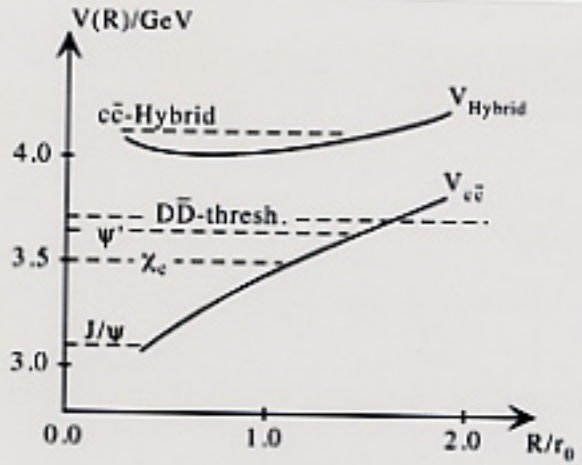

Figure 2.8. Potentials between static quarks at separation R, in units of r₀ ≈ 0.5fm, as derived from LQCD calculations (scaled from [21]). The $V_{c\bar{c}}$ curve represents the ground-state potential (no gluonic excitation) and corresponds to the conventional $c\bar{c}$ states J/ψ, χ_c, ψ', etc. The V_{Hybrid} potential originates from the first excited state of gluonic flux, giving rise to $c\bar{c}g$ hybrid states. The $c\bar{c}g$ ground state has the spin-exotic quantum numbers $J^{PC}=1^{-+}$ and is predicted to be a narrow state at about 4.2 GeV/c².

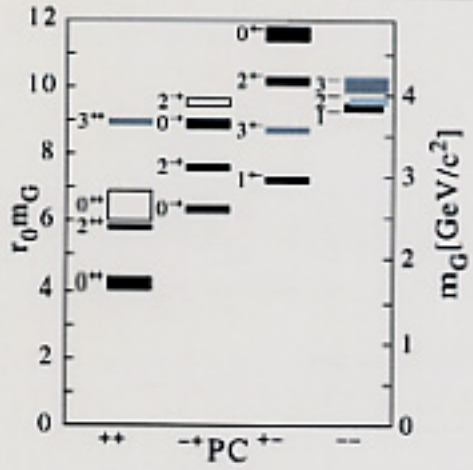

Figure 2.10. The glueball spectrum as derived from recent LQCD calculations [33], with 15 states in the mass region between 1.5 and 5.0 GeV/c². The relative mass uncertainties are indicated by the vertical extent of the boxes. For the $J^{PC} = 0^{++}$ ground state, a good experimental candidate has been found in $\bar{p}p$-annihilations, namely the $f_0(1500)$. All other glueballs are awaiting experimental discovery. The 2^{+-} state at 4.3 GeV/c² is of special interest, because it has exotic quantum numbers and can thus be easily distinguished from $q\bar{q}$ states.

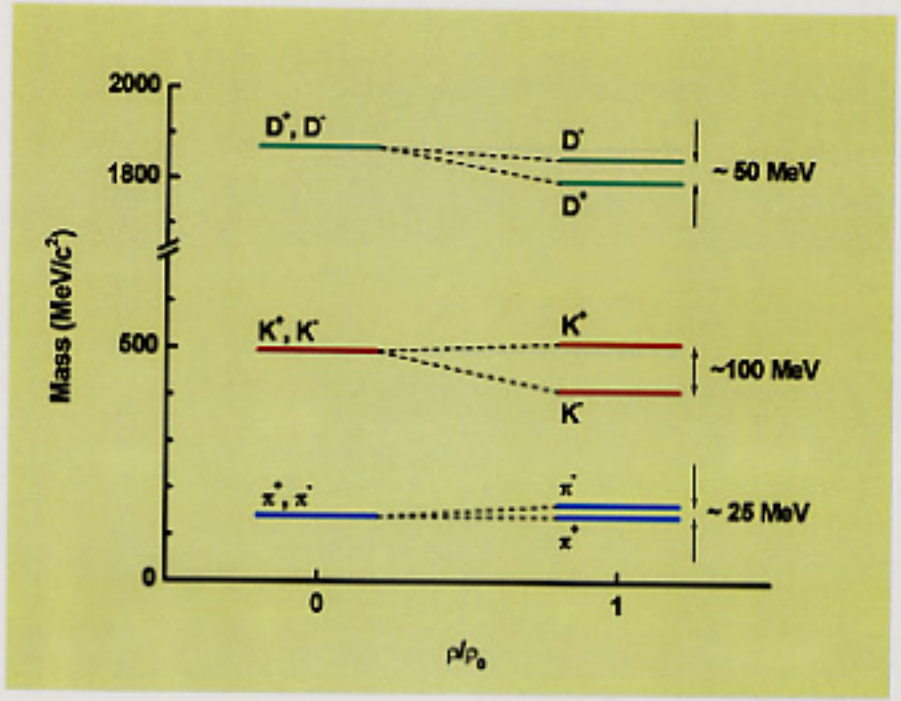

Figure 2.13. Schematic picture of hadron masses in vacuum and mass splitting in the nuclear medium at normal nuclear matter density as derived from [36,38,39].

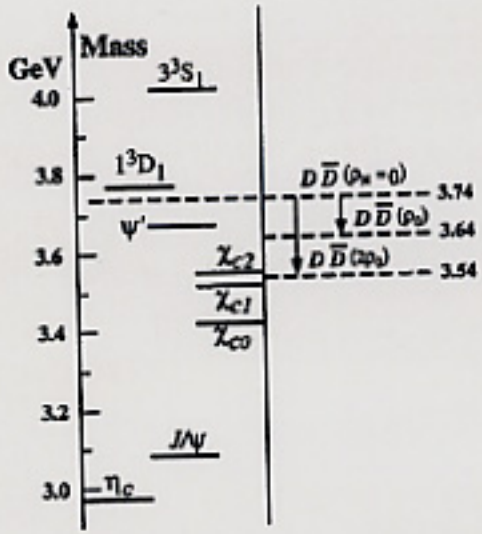

Figure 2.15. Charmonium states in comparison to the $\bar{D}D$ threshold in vacuum and in the nuclear medium at normal and twice normal nuclear matter density. The figure is taken from [41].

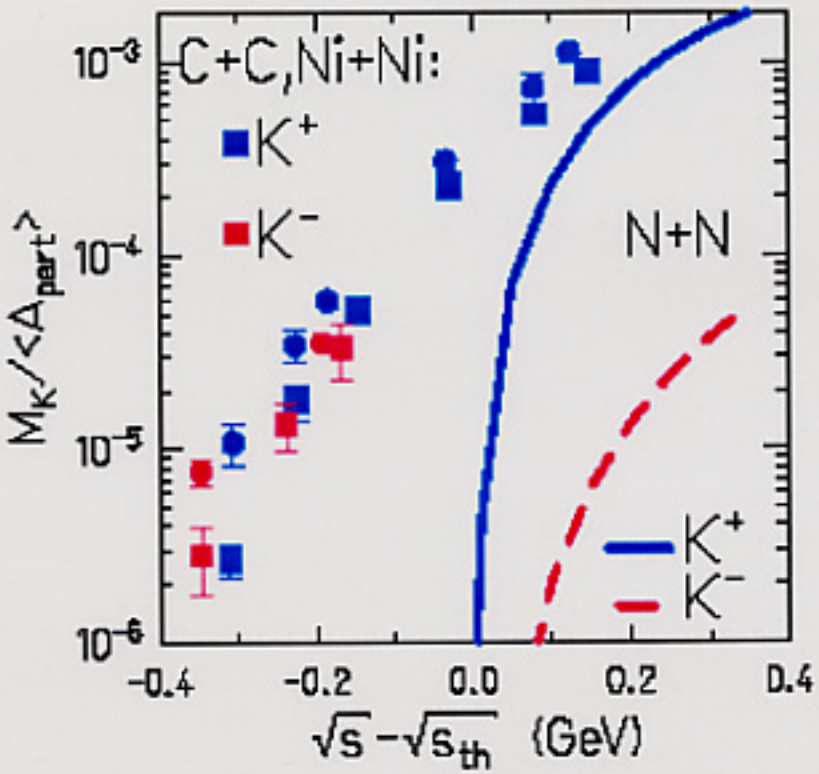

Figure 2.12. Excitation functions for K^+ and K^- meson production in heavy-ion collisions and elementary nucleon-nucleon reactions. The figure is taken from [38].

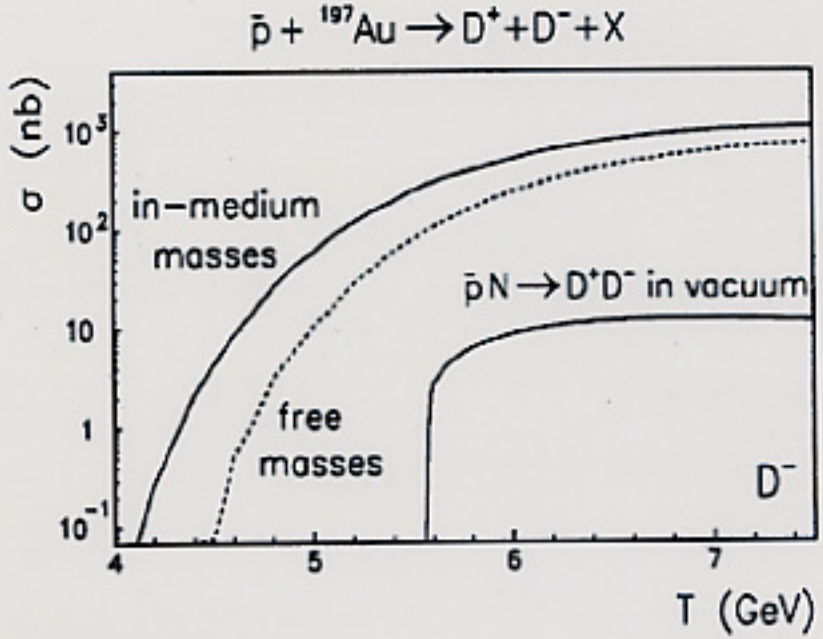

Figure 2.14. Total D meson pair production cross section in $\bar{p}$ annihilation on Au (upper curves) and on nucleons (lower curve) as a function of the antiproton energy. The cross sections for annihilation on Au were calculated for free (dashed curve) and in-medium (upper solid curve) masses of the D mesons. The figure is taken from [42].

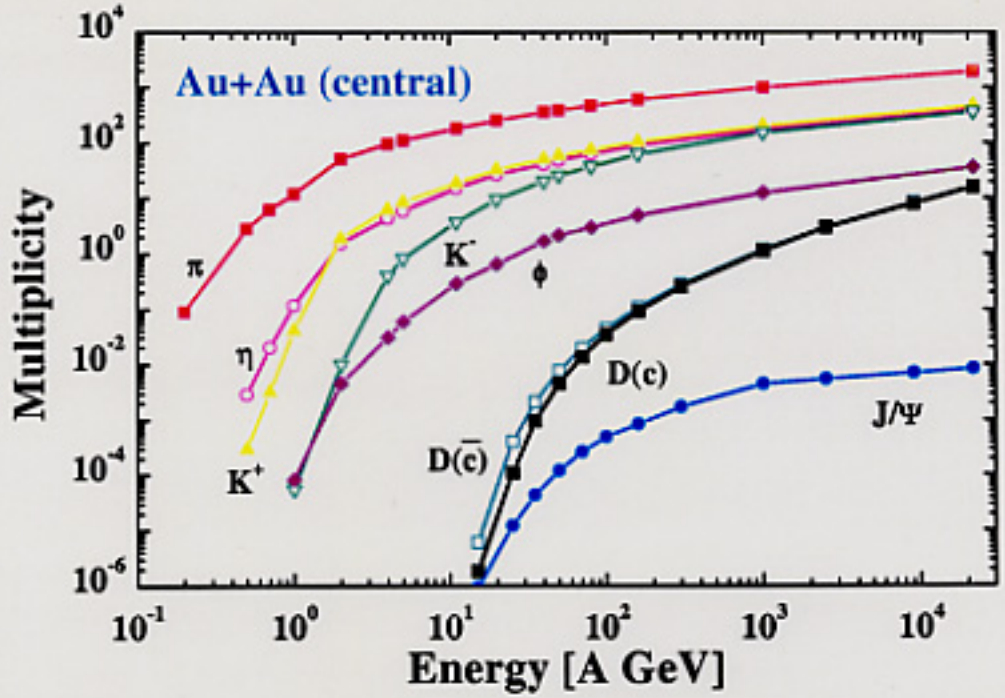

Figure 3.20: The average number of mesons produced per central Au+Au collision (multiplicity) as function of the incident beam energy. The calculation was performed with the HSD transport code. No in-medium mass modification was taken into account (taken from [51]).